PROCEEDINGS OF SPIE

SPIEDigitalLibrary.org/conference-proceedings-of-spie

The CONSORTIS 16-channel 340-GHz security imaging radar

Duncan A. Robertson, David G. Macfarlane, Robert I. Hunter, Scott L. Cassidy, Nuria Llombart, et al.

Duncan A. Robertson, David G. Macfarlane, Robert I. Hunter, Scott L. Cassidy, Nuria Llombart, Erio Gandini, Tomas Bryllert, Mattias Ferndahl, Hannu Lindström, Jussi Tenhunen, Hannu Vasama, Jouni Huopana, Timo Selkälä, Antti-Jussi Vuotikka, "The CONSORTIS 16-channel 340-GHz security imaging radar," Proc. SPIE 10634, Passive and Active Millimeter-Wave Imaging XXI, 1063409 (8 May 2018); doi: 10.1117/12.2304376

SPIE.

Event: SPIE Defense + Security, 2018, Orlando, Florida, United States

The CONSORTIS 16 channel 340 GHz security imaging radar.

Duncan A. Robertson*[1], David G. Macfarlane[1], Robert I. Hunter[1], Scott L. Cassidy[1], Nuria Llombart[2], Erio Gandini[2], Tomas Bryllert[3], Mattias Ferndahl[4], Hannu Lindström[5], Jussi Tenhunen[5], Hannu Vasama[5], Jouni Huopana[6], Timo Selkälä[6], Antti-Jussi Vuotikka[6]
[1] University of St Andrews, SUPA School of Physics & Astronomy, St Andrews, Fife KY16 9SS, Scotland
[2] Technical University of Delft, Delft, Netherlands
[3] Wasa Millimeter Wave AB, Gothenburg, Sweden
[4] GotMIC AB, Gothenburg, Sweden
[5] VTT Technical Research Centre of Finland Ltd., Oulu, Finland
[6] Global Boiler Works Oy, Oulu, Finland

ABSTRACT

We have completed a 16-channel 340 GHz 3D imaging radar for next-generation airport security screening under the European Union funded CONSORTIS (Concealed Object Stand-Off Real-Time Imaging for Security) project. The radar maps a 1 x 1 x 1 m^3 sense volume with ~1 cm^3 voxel resolution at multi-hertz frame rates. The radar has been installed in the CONSORTIS system enclosure and integrated with a passenger control system and command module. The full system will ultimately also incorporate a dual-band passive submillimeter wave imager and automatic anomaly detection software for reliable, ethical detection of concealed objects. A large data collection trial on targets of interest has been conducted to support the development of automatic anomaly detection software. Initial threat detection analysis indicates promising results against aviation-relevant objects including simulant dielectric threat materials.

Keywords: Radar, submillimeter wave, security, FMCW, imaging, concealed object detection.

1. INTRODUCTION

The continuing threat of terrorist attacks at airports and other mass transportation hubs is driving the development of new detection technologies which can offer improved performance and in particular improved throughput compared with existing security scanners. Recognizing this requirement, in 2011, the European Union solicited proposals to reduce the time needed for security checks while maintaining or increasing the level of detection under the Seventh Framework Programme (FP7) Topic SEC-2012.3.4.5-5 “Further research and pilot implementations of Terahertz detection techniques (T-Ray)”. Project proposals were expected to develop a prototype imaging system operating at a single or multiple sub/millimeter wave frequency, including frequencies above 300 GHz, which had to be safe for use on the general public and allow concepts of operation which respect privacy.

The CONSORTIS (Concealed Object Stand-Off Real-Time Imaging for Security) project[1] was funded under the above EU scheme between 2014 and 2017 with the aim of combining passive and active submillimeter wave imaging for next generation aviation security applications. The full CONSORTIS system combines a 340 GHz 3D imaging radar, a dual-band passive submillimeter wave camera, and automatic anomaly detection (AAD) software to ensure privacy. A passenger control system is used to coordinate passenger flow through the system and a command module maintains overall control of all the subsystems during system operation. The dual-mode approach, in conjunction with automatic anomaly detection software, aims to achieve higher detection performance whilst preserving the safety and privacy of staff and passengers. A primary goal of the project has been to achieve this enhanced security performance at a higher passenger throughput rate with the ultimate goal of having a walk-by system.

A CAD model of a passenger passing by the CONSORTIS system is shown in Fig. 1. The tower houses the radar above the radiometer and the passenger is imaged from one side as they pass by. Ultimately, two towers would be needed to provide full coverage but only one was built during the project.

*dar@st-and.ac.uk; phone +44 1334 467307; www.st-and.ac.uk/~mmwave

Passive and Active Millimeter-Wave Imaging XXI, edited by David A. Wikner, Duncan A. Robertson, Proc. of SPIE Vol. 10634, 1063409 · © 2018 SPIE
CCC code: 0277-786X/18/$18 · doi: 10.1117/12.2304376

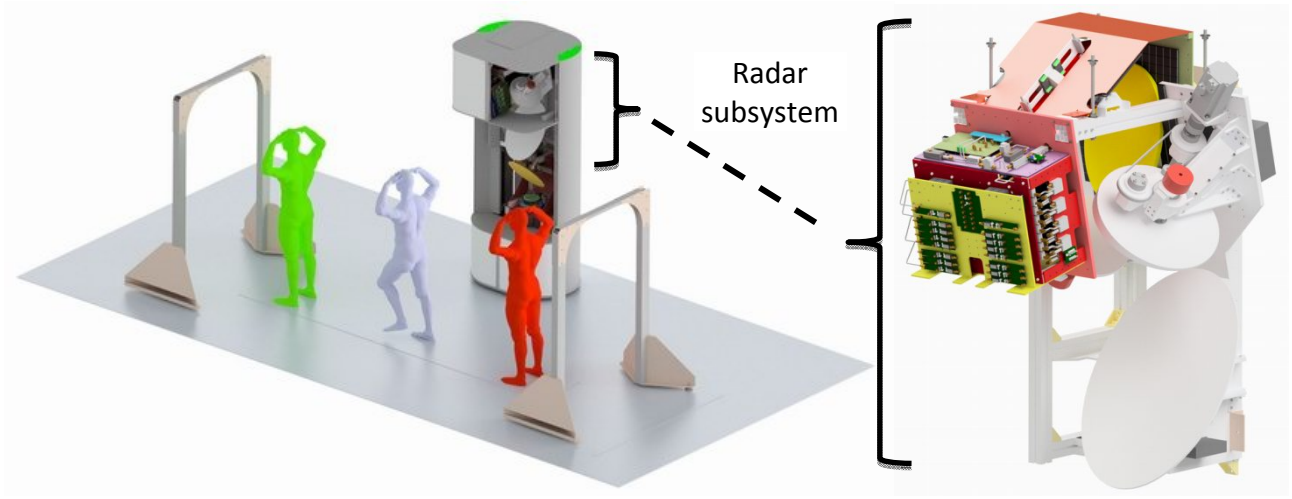

Figure 1. CONSORTIS system CAD model (left) showing one tower enclosure with radar mounted above radiometer. Passenger passes through passenger control system arches – key locations are entry (red), mid-way (grey) and exit (green). Radar subsystem CAD model (right).

The 340 GHz radar subsystem development has been previously reported[2] and this paper presents results obtained during the completion and characterization of the radar. The radar has been integrated into the CONSORTIS system along with the passenger control system and the command module. Data collection trials were conducted to gather statistically relevant data on a range of targets, subjects and clothing types and some example imagery is presented here.

2. RADAR SUBSYSTEM OVERVIEW

The CONSORTIS radar subsystem[2] uses 16 homodyne 340 GHz transceivers disposed in a linear sparse focal plane array (FPA) combined with high speed mechanical beam scanning. It images a 1 x 1 x 1 m^3 volume with ~1 cm^3 voxel resolution at a frame rate of 7 Hz. A direct digital synthesis (DDS) based wideband chirp generator with an output at ~10 GHz drives the solid state frequency multiplier transceivers which cascade x8 MMIC and x2-x2 Schottky diode doublers. The transmitted chirp bandwidth is 30 GHz yielding 0.5 cm range bins. A critical enabling technology in achieving such a high channel count FPA is the use of self-mixing multipliers as the final stage – the final transmit doubler also acts as a mixer on receive, with the baseband IF signal extracted via the bias line[3]. This technology greatly simplifies the homodyne architecture and excludes the need for external transmit-receive duplexing components. The slight degradation in sensitivity compared with a homodyne receiver using a dedicated mixer is well tolerated in this short range application.

The radar signals from the transceiver array are coupled to free-space using smooth-walled spline profile feedhorns and focused to sixteen ~1 cm diameter spots which are vertically aligned in the focal plane with a spacing of 6 cm. A pair of mirrors in a Dragonian configuration provides the focusing. Azimuth beam scanning is performed by a Lissajous scanner comprising a pair of counter rotating, canted plane mirrors which cause each focal spot to trace out a long thin figure-of-eight. Elevation scanning, to fill in the scan pattern, is achieved by reciprocating the Dragonian primary mirror up and down for every pair of frames.

A block diagram of the radar architecture is shown in Fig. 2 alongside a ray diagram depicting the key optical components. The raw IF signals from the transceivers are bandpass filtered to select the 1 m range swath at the working distance (~2.4 m), amplified and frequency translated down to a 1 – 6 MHz baseband in a 16 channel analog range-offset downconverter circuit. Received signals are sampled by a 16 channel ADC and then FMCW processed by FFT to form range profiles for every line of sight in the scan pattern. The field of view (FoV) can be steered in azimuth as passengers walk past using a large plane pan mirror which completes the optics. The radar views the subject from a slightly elevated

position with a look-down angle of 12.5°. As the FoV is steered by the pan mirror the approximately cubic sense volume rotates by the pan angle.

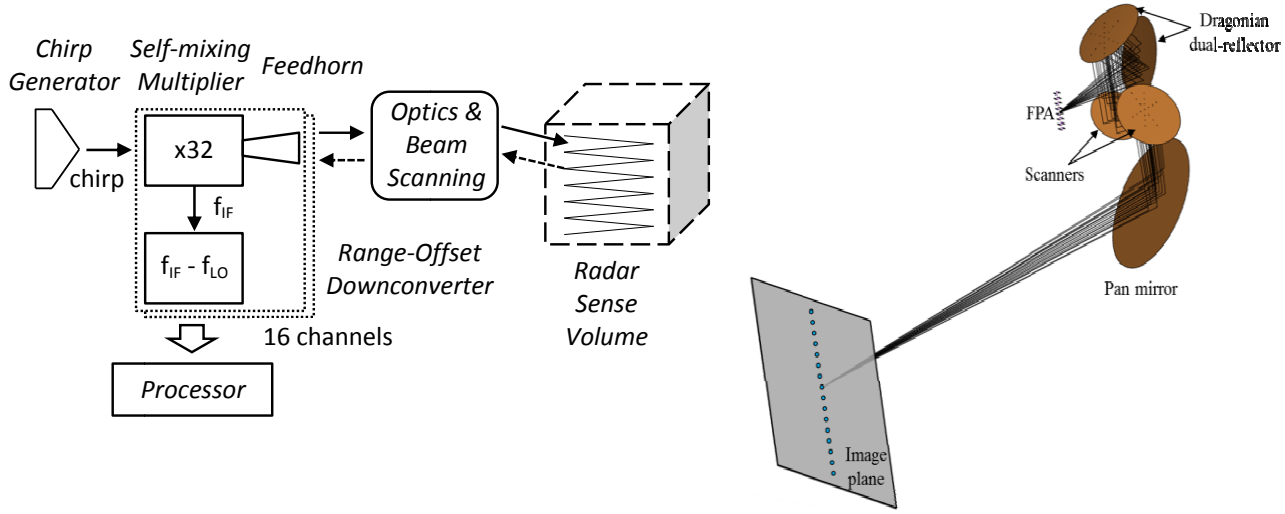

Figure 2. CONSORTIS radar subsystem block diagram (left) and optical element ray trace diagram (right).

3. RADAR SUBSYSTEM CHARACTERISATION & OPTIMIZATION

Subsequent to the completion of the hardware build, the radar was subject to extensive characterization of its radar (range and amplitude) and spatial responses. To compensate for imperfections in the radar response and non-ideal scan pattern, corrections were applied to maximize the fidelity of the resulting 3D imagery. This process of characterization and optimization is summarized in the following section.

3.1 Radar response characterization

The security imaging application requires a fine range resolution in order to be able to reveal thin objects and resolve them from layers of clothing. The range resolution is nominally set by the chirp bandwidth but, as is typical of wide bandwidth submillimeter wave radars, it is usually degraded to some extent by group delay and amplitude variations across the chirp bandwidth[4, 5]. However, it is well known that these effects can be compensated for over a limited range of ranges by measuring a reference point target and applying an amplitude and phase correction to the raw received signal, prior to FFTing.

The raw radar range profile was measured successively for all 16 channels using a well isolated sub-beamwidth point target (a square trihedral with 4mm edge length) positioned at the respective focal spots in the image plane. Amplitude and phase corrections were derived for each transceiver and subsequently applied to the input raw data streams. An example range profile showing the raw and calibrated responses is shown in Fig. 3 (left). The raw range profile is already quite clean given the wide 30 GHz chirp bandwidth, with sidelobes only appearing below -20 dBc. This is testament to the low level of group delay and amplitude variation in the chirp generator and transceiver components. The calibrated range profile exhibits no residual range sidelobes and is transform limited down to the system noise floor at -50 dBc. The noise floor pedestal appears due to the receive bandpass filter which defines the 1 m range swath of the target volume (20 to 120 cm on the x axis). The calibrations are different for each transceiver due to slight differences in the characteristics of each unit but the calibrations have been found to be very stable over periods of weeks and frequent recalibration is not necessary.

The range bin width was confirmed using a two-target test in which two sub-beamwidth point targets were positioned in the same line of sight to a transceiver but separated in range by exactly 10 cm. The range profile of this two-target test is shown in Fig. 3 (right). The two peaks are very clearly resolved and are exactly 20 range bins apart, confirming that the range bin width is 0.5 cm. No oversampling or zero-padding is used in these range profiles.

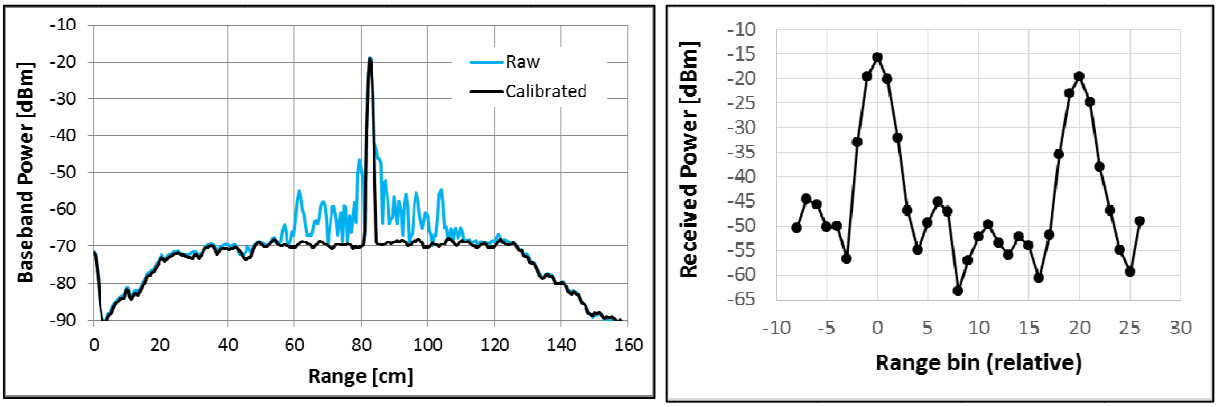

Figure 3. Range profile (left) showing raw and calibrated response from a point target – the calibrated response is transform limited over a 50 dB dynamic range. Two-target test range profile (right) for two point targets separated by 10 cm – the peaks are exactly 20 range bins apart, confirming the range bin width of 0.5 cm.

A key parameter of interest when characterizing a multi-pixel imager is the amplitude balance between channels. The amplitude performance of a given transceiver can be expressed by defining a figure of merit, FOM, equal to the ratio of output power (typ. 0 dBm) to conversion loss (typ. -18 dB). This quantity maps directly into the radar equation for each transceiver so can be used to assess channel balance across the array. In the process of FMCW deramping, the FOM variations across the chirp bandwidth are effectively averaged out so the mean value of FOM can be used to indicate the overall effect on the received IF signal. The mean values of FOM for all channels fall within the range -19.5 to -16.4 dB. Such a small ~3 dB variation shows there is excellent channel balance across the array. This is attributed to the tight tolerances achieved in the performance of the frequency multiplying transceivers.

3.2 Optics characterization

The spatial beam quality of each radar pixel is governed by the optical quality of the 5 mirror elements in the beam path but dominated by the effect of the curved focusing mirrors in the Dragonian pair. The double disc and pan mirrors all have nominally planar surfaces. The two 385 x 290 mm focusing mirrors, shown in Fig. 4, use complex mechanical designs in combination with an ultra-stable grade of aluminum and a careful machining process to achieved the desired doubly-curved profiles. The rear faces of the mirrors have arrays of stiffening webs to maintain dimensional stability whilst reducing weight. In the case of the primary mirror, which has to reciprocate at several hertz, the design achieves low mass (1.3 kg) and a perfect balance about the pivot axis is achieved through subtle contouring of the pockets between the stiffening ribs.

Figure 4. Dragonian focusing mirrors showing stiffening ribs on rear of static secondary mirror (left) and reciprocating primary mirror (right). The focusing surfaces conform to the design profile within ±30 μm (~λ/30).

The optical beam quality was assessed with static radar beams (beam scanner stationary) by rastering a point target across the beam at the plane of interest whilst collecting the reflected power. A computer controlled two-axis beam scanner was used to scan in a plane inclined at -12.5° from the vertical, to be normal to the primary beam axis. The point target was mounted on the tip of a plastic rod radially aligned towards the radar. Measurements were restricted to the

range bin containing the point target to isolate it from reflections at greater range due to the beam scanner itself which were well separated due to the length of the plastic rod.

Measurements of the focal spots of all 16 transceivers were made in various positions in the FoV (set by adjusting the beam scanning mirrors) and at different range planes (selected in the range profiles). An example measured two-way (radar) 2D beam scan of the focal spot for transceiver +1 (just above FoV centre) at nominal range center (mid plane) is shown in Fig.5 (left). The corresponding simulation, obtained using GRASP is shown in Fig. 5 (middle) and principal axis cuts through measured and simulated data are shown in Fig. 5 (right).

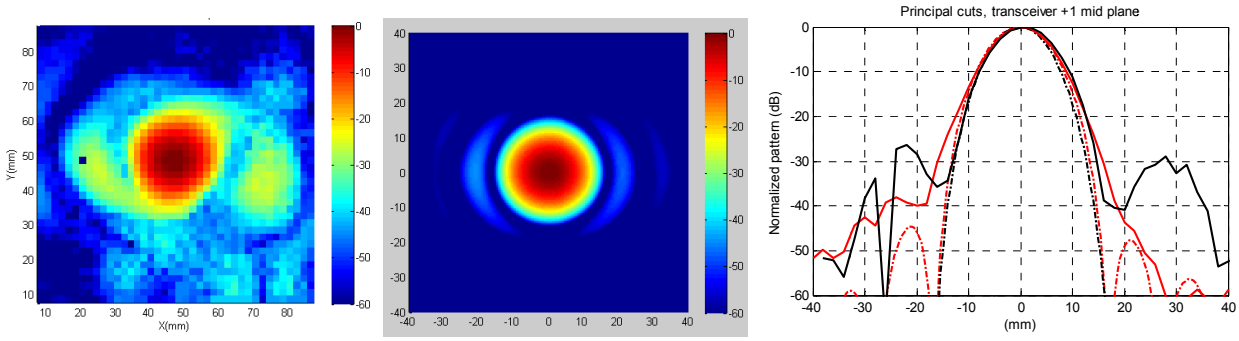

Figure 5. Measured 2D two-way (radar) beam scan of transceiver +1 at mid plane (i.e. range center) (left), corresponding simulation (middle) and measured versus simulated principal plane cuts (right).

These results confirm that the -3 dB radar spot size is ~1 cm as designed, with good circular symmetry. Overall, the agreement with simulation is very good for the main lobe to below -25 dB. Sidelobes at the -27 dB level are evident in the azimuthal direction, slightly higher than predicted. The good beam quality and agreement with simulations verifies the dimensional accuracy of the focusing mirror profiles.

3.3 Scan pattern corrections

The 1 x 1 m^2 field of view is sampled by 144 x 100 lines of sight (elevation x azimuth). Range profiles measured for each line of sight in a frame are triggered by a shaft encoder on the double-disc scanner motor whose spacing is proportional to the cosine of the shaft angle. This ensures the azimuth points are equally sampled in angle. With 16 transceivers disposed vertically, each transceiver covers 9 lines per frame in elevation, scanned by the reciprocating mirror. The elevation scan drive waveform (nominally a triangle wave) is clocked by a conventional encoder also mounted on the double-disc scanner motor shaft. The motor undergoes 4.5 rotations to complete the 9 line scans of one frame. In practice, the reciprocating mirror does not follow the drive waveform perfectly so the actual elevation scan pattern is distorted. Due to the combination of the reciprocating elevation scan and the figure-of-eight azimuth scan, up frames and down frames have slightly different non-uniform sampling patterns. The data processing and display has to take account of these non-ideal scan patterns in order to present a geometrically accurate view of the scene. Fig. 6 shows simulated azimuth scan patterns of the up and down frames (left) and the measured elevation scan pattern versus the triangular input drive waveform (right), measured at a frame rate of 7 Hz.

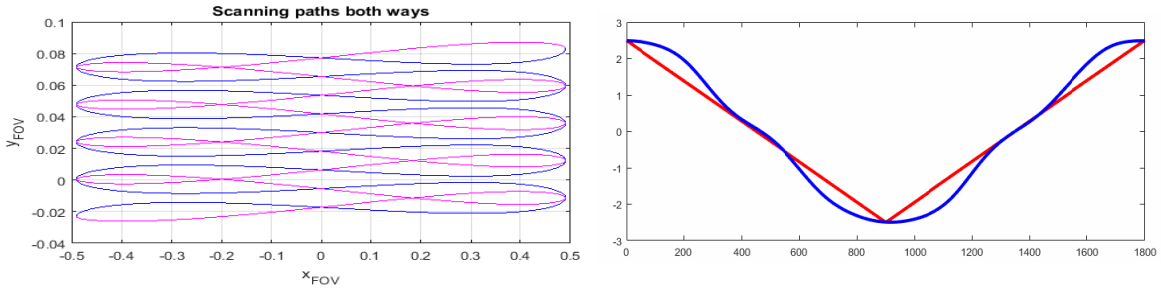

Figure 6. Simulated azimuth scan patterns due to Lissajous scanner (left) for one transceiver for up frame in pink and down frame in blue, assuming a linear elevation scan. Note the vertical axis is very much enlarged; both axes in meters. Measured elevation scan pattern at 7 Hz frame rate (right) with triangular mirror drive waveform in red and actual measured position in blue, showing nonlinearity of the reciprocating mirror motion.

The radar was designed to operate at a 10 Hz frame rate and both the mechanical beam scanning and radar processing achieve that speed. However, in practice, the frame rate has had to be restricted to 7 Hz due a timing synchronization latency in the trigger electronics which control the start of each acquisition. Operating at frame rates above 7 Hz causes alternative left-to-right and right-to-left lines to become displaced. A fairly simple modification to the trigger electronics would allow the imaging speed to be increased to the full frame rate of 10 Hz.

The azimuth scan pattern is derived from the geometrical ray trace of the Lissajous scanner whilst assuming a perfectly linear elevation scan. Since there are 9 left-to-right and right-to-left lines per frame whose elevations advance progressively that the scan patterns are obviously different for up and down frames. The measured elevation scan pattern was determined using Hall sensors which measured the deflection of the linear motor shafts that drive the reciprocating mirror up and down. It is clear that the mirror motion does not perfectly follow the triangular drive waveform and this is due to mechanical resistance in the drive coupling and air resistance. By combining the azimuth and elevation scan pattern distortions it is possible to assign a geometrically accurate pointing angle to each line of sight in the image.

Currently, raw data is processed and displayed without scan pattern corrections in real-time on the control PC using multi-threaded C code with the radar image presented as a 2D projection of the data cube, color coded by maximum reflected power. The scan pattern corrections are then applied offline in MATLAB accounting for the differences in up and down frames. The true pointing angles of each pixel are not spaced equally in azimuth and elevation so the final image is interpolated onto an equally spaced rectilinear grid for subsequent processing and analysis. Fig. 7 shows one frame, color coded by maximum intensity, which compares the raw image indexed by encoder position which is geometrically incorrect, a dot plot indicating the true positions of each pixel, and the final interpolated image which has correct geometry. The image quality is noticeably improved after the scan pattern corrections are applied.

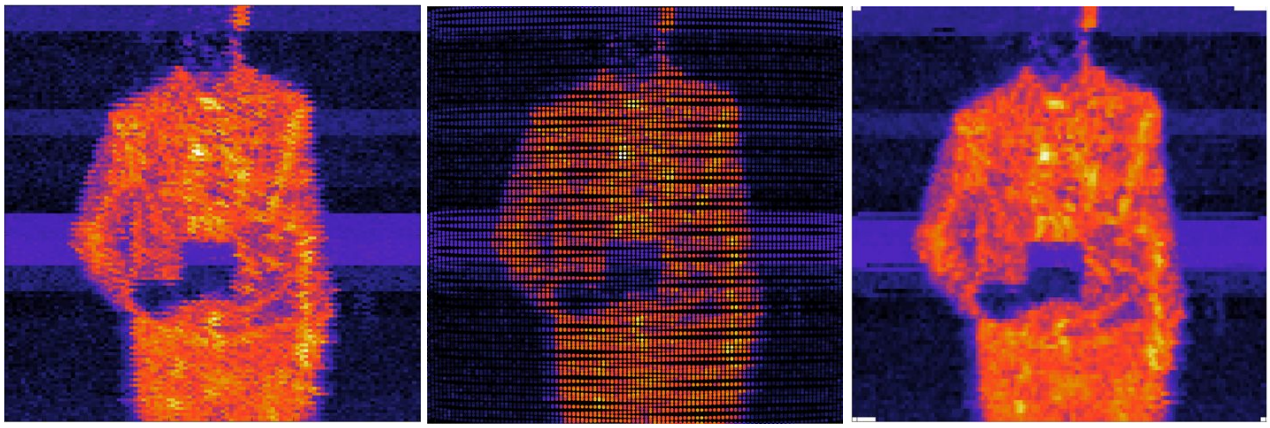

Figure 7. Single frame color coded by maximum intensity comparing: (left) raw image indexed by encoder position showing geometrical errors especially at edges, (middle) dot plot indicating the true position of each pixel in the scan pattern, and (right) interpolated image with the correct geometry after application of the scan pattern corrections. Intensity color scale covers 60 dB. Range extent limited to 35 cm around the torso to reduce data saving burden, hence the face and hand are slightly clipped in intensity.

4. DATA COLLECTION EXAMPLE IMAGERY

The radar subsystem was mounted into the CONSORTIS system enclosure and Fig. 8 shows the radar fitted in the upper part of the CONSORTIS tower with the pan mirror visible. The space below the radar is for the passive radiometric imager. The radar subsystem itself is shown in close up, in which the radar electronics and optomechanical components for the beam scanning mechanism can be clearly seen. The radar dimensions are 73 x 91 x 115 cm and the estimated weight is ~130 kg. The radar subsystem (radar head plus control PC) is all powered by a dedicated power supply located at the bottom of the equipment rack to the right of the system tower. The radar power consumption is <750 W.

The radar was then integrated with the Command Module (CM) and the Passenger Control System (PCS) to enable automatic system testing and data collection. The PCS uses a suite of sensors and indicator lights mounted on two archways to control passenger flow through the system. A Microsoft Kinect sensor on the exit arch detects the presence of a passenger entering the system through the entry arch and the CM automatically sequences the process of passenger flow control and radar data acquisition. In the current concept of operation, the radar is designed to acquire a burst of

frames at the entry and exit positions where the passenger is paused briefly, waiting for the stop/go indicator lights. The CM instructs the pan mirror to steer to the entry and exit points appropriately and for the radar to acquire the relevant data, which is then available on the data bus for subsequent processing.

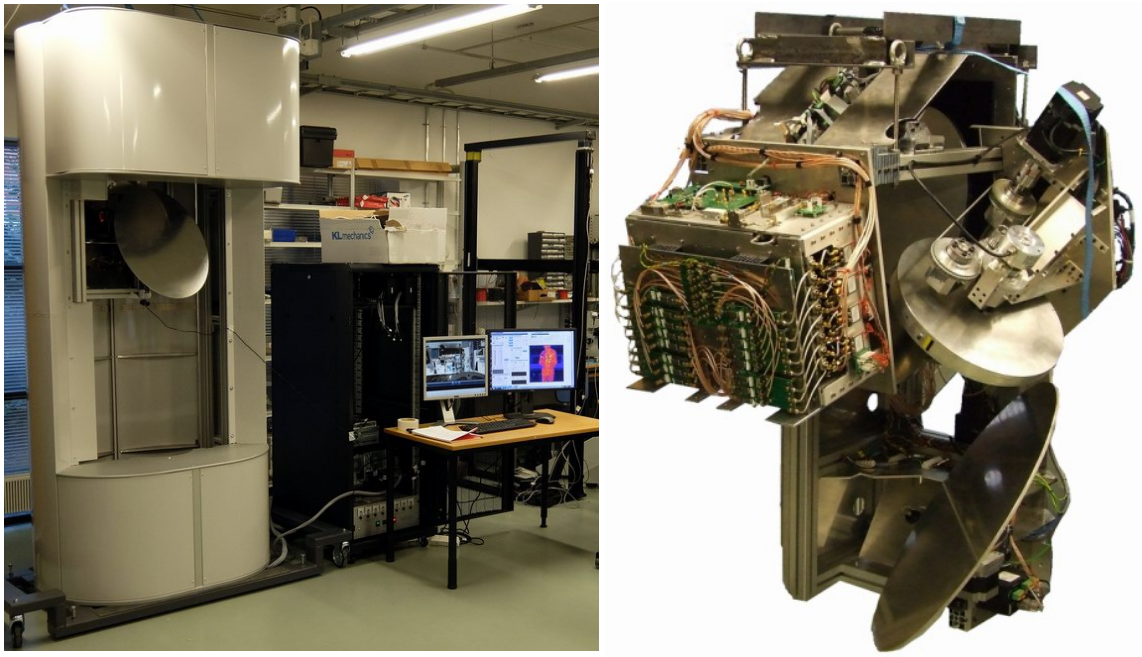

Figure 8. CONSORTIS tower deployed at VTT, Espoo, Finland, with radar subsystem mounted inside and control PC to right hand side (left). Radar subsystem close up (right).

When the pan mirror steers, the FoV rotates by the pan angle, as noted above. Fig. 9 illustrates this effect with CAD views of a mannequin at the entry and exit positions with the FoV overlaid, plus example radar intensity images of a real person from these viewpoints. The radar thus obtains ¾ views of the person from the front and back as they pass through the system. As mentioned previously, a full deployment would require two towers to view the subject from both sides.

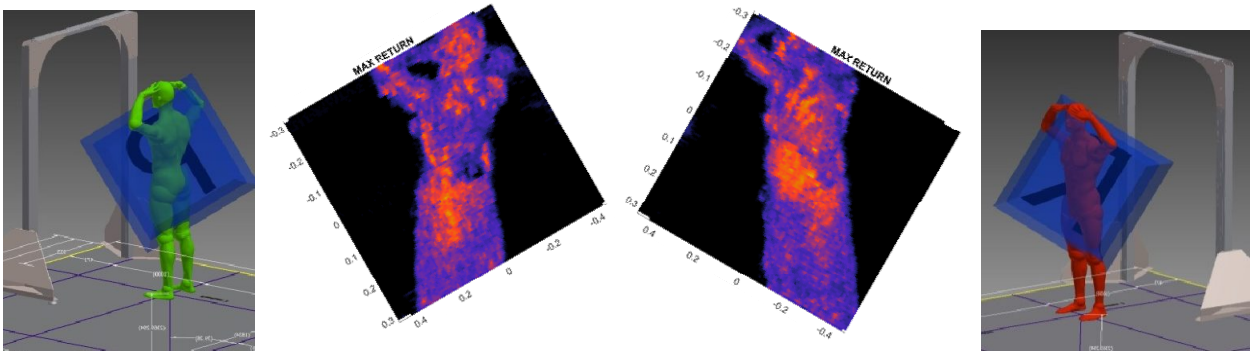

Figure 9. FoV rotation during panning showing entry point (right) and exit point (left) as the subjects passes from right to left through the system with CAD models and example radar intensity images of a person.

A considerable amount of data has been gathered with the radar to assess its performance. A data collection trial was conducted which acquired >1000 data runs in an operationally realistic scenario. The tests covered a range of subjects, threat items, threat locations and clothing. Weapons plus real and simulant aviation-relevant dielectric threat materials were used. Detailed results of the trial are beyond the scope of this publication but a few examples can be given to illustrate the imagery acquired.

Since the radar collects bursts of 3D data it can be prepared for analysis and presentation in different ways, although not all of them appear optimally on a 2D screen or static page. Two example display formats which we use frequently are (i)

color coding by maximum intensity per line of sight, and (ii) color coding by range to last surface. The former is very simple to calculate and interpret but is often dominated by external surface reflections. The latter uses the fine range resolution of the radar to reveal objects underneath clothing layers. Note that in both cases, because the information is encoded in a color scale, they are subject to human perception differences. Alternative presentations could be point clouds, surface reconstructions, contour plots, etc. Two example data sets are shown in Figs. 10 and 11 using the two color codings described above. These are single frames of radar data and include the range and scan pattern corrections.

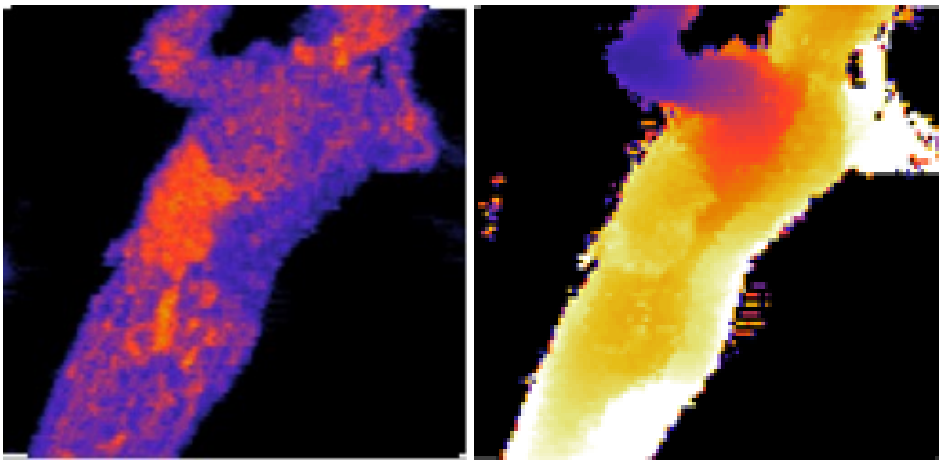

Figure 10. Subject at exit point with large conformal dielectric threat simulant attached to their side, under clothing. Color coded by maximum intensity (left) and by range to last surface (right). Color scale covers 60 dB.

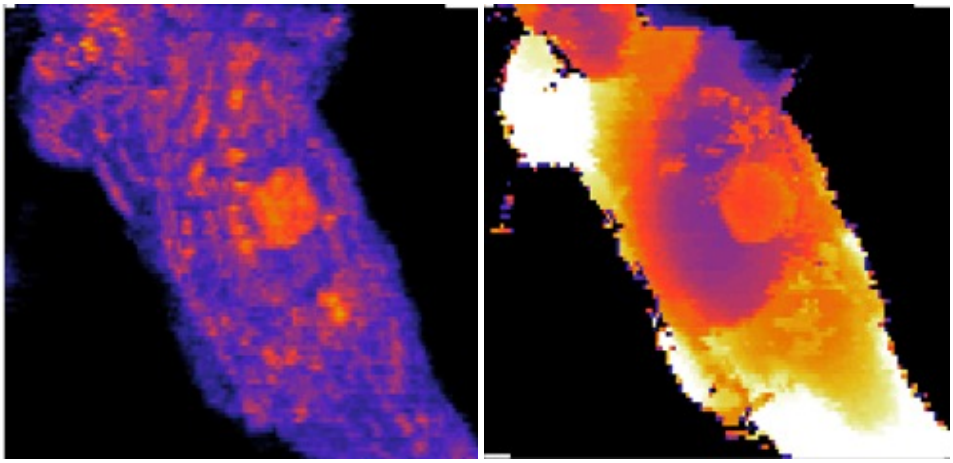

Figure 11. Subject at entry point with small dielectric threat simulant attached below their armpit, under clothing. Color coded by maximum intensity (left) and by range to last surface (right). Color scale covers 60 dB.

In both examples shown here, the dielectric threat simulants appear clearly in both display presentations. However, it should be noted that (as is well known) the maximum intensity display can be sensitive to surface effects from clothing and speckle which may mask or even confuse the detection of a concealed threat. In contrast, the range to last surface effectively sees through the clothing and reveals the contours of the concealed object underneath. A robust automatic anomaly detection algorithm is likely to combine the analysis of more than one data presentation.

The trial data have been used to support the development of AAD algorithms by project partner FOI, Sweden, and to derive preliminary receiver operating characteristic (ROC) curves for the detection performance of the radar against different threats. Initial ROC curves have been derived using human operator classification of various 2D and 3D data presentations similar to that shown above and have yielded some very promising results. Work is ongoing to develop a fully automatic detection scheme using AAD algorithms.

From the large number of trial images obtained it became evident that a human operator can easily distinguish gender differences and can even identify individuals after repeated imaging. This illustrates the high fidelity of the radar but further highlights the need for automatic image analysis to remove human observation and maintain passenger privacy and ethical operation.

5. DISCUSSION & CONCLUSIONS

The EU FP7 CONSORTIS project has successfully completed the development, characterization and testing of an advanced submillimeter wave radar imager for next-generation airport security applications. The 340 GHz 3D imaging radar combines a sparse array of 16 radar transceivers with high speed mechanical beam and real-time processing to map a 1 x 1 x 1 m^3 sense volume with ~1 cm^3 voxel resolution at multi-hertz frame rates. Self-mixing multiplier technology has been crucial in achieving a large focal plane array of 16 channels without the need for external duplexing components. We believe this is the highest channel count submillimeter wave radar reported to date.

To optimize the radar image fidelity, thorough characterization of the range and spatial responses was undertaken from which corrections were derived and applied to the raw data. The radar range profile, whilst quite clean in raw form due to the high performance chirp generator and frequency multiplying transceivers, becomes transform limited down to the system noise floor with a range bin width of 0.5 cm. The range calibration is different for each channel and has been found to be stable over periods of weeks, avoiding the need for frequent recalibration.

The beam profile was characterized at multiple positions in the sense volume using a scanned point target. The -3 dB radar spot size was confirmed to be ~1 cm as designed and measured beam profiles agree well with simulations, validating the quasi-optical design and reflecting the high precision manufacture of the focusing mirrors whose surfaces conform to their design profiles to within ~$\lambda/30$.

The mechanical beam scanning arrangement exhibits non-uniform sampling scan patterns in azimuth (figure-of-eight) and elevation (non-linear) which have been characterized. Scan pattern corrections have been derived which account for these distortions and are applied to the output data to yield geometrically accurate images.

The radar subsystem has been mounted in the CONSORTIS tower enclosure and integrated with the Passenger Control System and Command Module. In the full system, the radar will be joined by a dual-band passive submillimeter wave imager. Operating fully automatically, under control of the CM and PCS, the radar has been used to collect >1000 data sets on realistic threat scenarios involving different people, threat items, threat locations and clothing. Weapons plus real and simulant dielectric threat materials were used.

The example imagery demonstrates the high volumetric resolution of the radar and its ability to reveal small, even dielectric, objects concealed under clothing. Video sequences obtained at 7 Hz frame rate demonstrate the temporal fidelity of the radar imagery, providing multiple looks at targets which may vary with aspect angle. Initial ROC curves have been derived from human classification of 2D and 3D data presentations which show very promising results. Work is ongoing to develop a fully automatic detection scheme using AAD algorithms. The need for AAD algorithms to ensure passenger privacy and ethical operation has been underscored by the level of detail visible in the imagery.

The CONSORTIS project has successfully demonstrated a 340 GHz radar imager within a prototype security screening system that is capable of acquiring high resolution 3D imagery at multi-hertz frame rates which can resolve threat objects concealed under clothing. This submillimeter wave radar technology, when combined with automatic anomaly detection software, will be suitable for future high throughput aviation security screening applications.

6. ACKNOWLEDGEMENTS

Part of the research leading to these results has received funding from the European Union Seventh Framework Programme (FP7/2007-2013) under grant agreement no. 312745. The authors are very grateful to all our colleagues in the CONSORTIS project for their dedicated support and collaboration, in particular those from VTT, FOI and Finavia who contributed substantially to the system integration and data collection tasks.

REFERENCES

[1] CONSORTIS website: http://consortis.eu/

[2] Robertson, D.A., Macfarlane, D.G., Hunter, R.I., Cassidy, S.L., Llombart, N., Gandini, E., Bryllert, T., Ferndahl, M., Lindström, H., Tenhunen, J., Vasama, H., Huopana, J., Selkälä, T. & Vuotikka, A-J., "High resolution, wide field of view, real time 340 GHz 3D imaging radar for security screening," Proc. SPIE 10189, 101890C, 1-9 (2017)

[3] Dahlbäck, R., Bryllert, T., Granström, G., Ferndahl, M. Drakinskiy, V. and Stake, J., "Compact 340 GHz homodyne transceiver modules for FMCW imaging radar arrays," IEEE MTT-S International Microwave Symposium (IMS), 1 – 4 (2016)

[4] Cooper, K.B., et al., "THz Imaging Radar for Standoff Personnel Screening," IEEE Trans. Terahertz Science and Technology, 1 (1), 169 – 182 (2011)

[5] Grajal, J., Badolato, A., Rubio-Cidre, G., Ubeda-Medina, L.; Mencia-Oliva, B., Garcia-Pino, A., Gonzalez-Valdes, B., and Rubinos, O, "3-D High-Resolution Imaging Radar at 300 GHz With Enhanced FoV," IEEE Trans. Microwave Theory Tech., 63 (3), 1097-1107 (2015)